FM2002

Deep Structure of the Shelf and Slope of the Northern Gulf of Mexico

Part B: An Ocean-Bottom Seismograph - Air Gun Experiment

by

Joseph O. Ebeniro, Dale S. Sawyer, Yosio Nakamura,
F. Jeanne Shaub and William P. O'Brien, Jr.

Final Technical Report

Submitted to Sponsors

December 12, 1985

Institute for Geophysics
The University of Texas at Austin
4920 North I.H. 35
Austin, Texas 78751

University of Texas Institute for Geophysics Technical Report No. 41

SUMMARY

We have conducted a large-offset seismic experiment in the northern Gulf of Mexico, offshore of East Texas, using large-capacity air guns and ocean-bottom seismographs. The purpose of the experiment was to map the deep sedimentary and crustal structures underlying the thick sedimentary cover which also included many salt intrusives. Five lines, each approximately 90 km long with four to five OBS's, were shot over an area which extended from mid-shelf at about 50 m water depth to the continental rise just beyond the Sigsbee Escarpment at about 3100 m water depth.

The acquired data were first analyzed and interpreted using standard techniques: layer solutions from phase velocities and intercept times of refracted arrivals, interval velocities from moveout of pre-critical reflections and inversions of data transformed to the tau-p domain by slant-stacking. For several of the lines, however, the structures were too complex to yield much information using these one-dimensional analyses. In these cases, we used two-dimensional ray tracing to define shallow structures as well as the depths to the deeper refractors.

The entire study area is covered with sediments 13 to 15 km thick. Various types of salt features are found within the sediments in the slope area ranging from deeply buried salt and diapirs under the inner slope to shallow, thin, allochthonous salt bodies under the outer slope. The crust shows considerable lateral variation in velocity and thickness. Oceanic crust typical of the central Gulf of Mexico underlies the continental rise south of the Sigsbee Escarpment. Under the slope and the shelf, the crust is thicker, probably representing extended continental crust. There is, however, crust of nearly oceanic thickness under the mid slope, suggesting an additional locus of extension during rifting. The crust thickens rapidly under the shelf, presumably reaching nearly normal continental thickness north of the coast line.

INTRODUCTION

Wide areas of the northern Gulf of Mexico are underlain by thick sediments transported from the vast expanse of the North American continent since Late Jurassic time. Because of this thick sedimentary cover and also of numerous salt deposits that are found in many areas of this region, it is difficult, and often impossible, to probe the underlying crustal layers using conventional seismic refraction techniques *[Ewing et al.*, 1960; *Antoine and Ewing*, 1963] or modern seismic reflection techniques commonly used in the petroleum industry.

In order to acquire seismic data relevant to the deep crustal structure of the northern Gulf of Mexico, we have been conducting a series of large-offset seismic experiments using ocean-bottom seismographs (OBS) and large-capacity air-guns. Using OBS, seismic lines may be extended to very large offsets, enabling us to obtain refracted and wide-angle reflected arrivals from deep layers. The relative quiescence of the ocean floor compared with the sea surface is advantageous for detecting weak seismic signals. Air-gun sources provide more accurately timed, uniform and spatially dense sources than explosive sources commonly used in earlier seismic refraction surveys.

In late 1983, the Institute for Geophysics of the University of Texas at Austin and the U. S. Geological Survey conducted a field study in the Gulf of Mexico off the eastern Texas coast (Fig. 1). The study was sponsored by a group of three U. S. oil companies and was performed in two parts: Part A - a two-ship multichannel expanding-spread-profile (ESP) seismic experiment and Part B - an OBS experiment. For both parts of the study, we used large-capacity air guns for seismic sources. Both experiments covered the same lines. This report describes the results of the Part-B experiment.

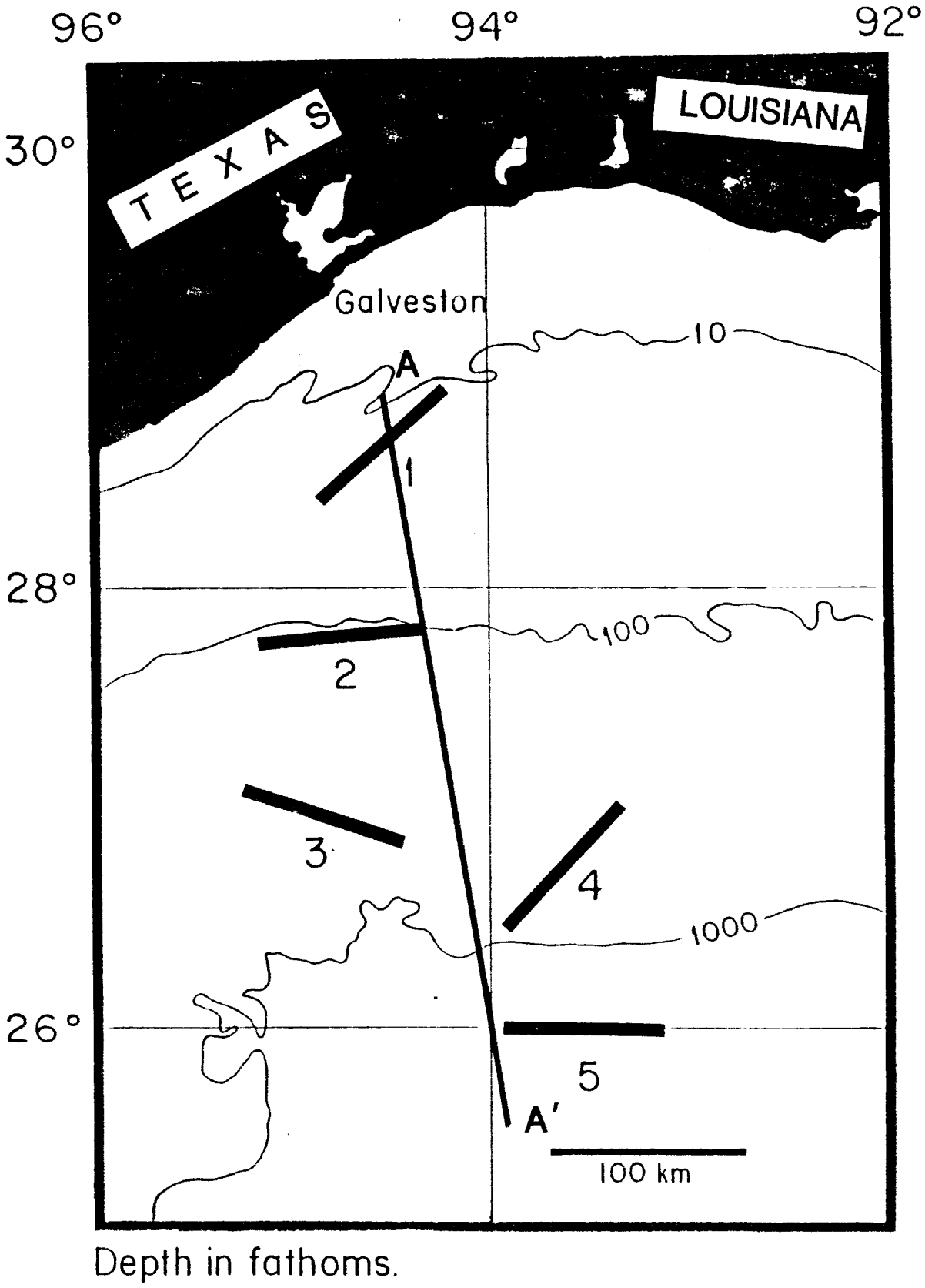

Fig. 1. Location map of the five seismic lines, 1 through 5, shot during the experiment. Line A-A' refers to a cross section discussed later.

FIELD EXPERIMENT

Seismic Lines

The five seismic lines, Fig. 1, were selected by scientists at UTIG in consultation with the sponsors. One of the main concerns for the selection was to avoid complicated salt structures as much as possible so that good depth penetration of seismic waves could be achieved. Each line is approximately 90 km long with four or more OBS's as receivers and about 1200 air-gun shots as signal sources along each line. A few sonobuoys were deployed on each line for supplementary information. Coordinates of the line end points and locations of the successful OBS's are listed in Tables 1 and 2, respectively.

The geometry of the seismic lines, Fig. 2, is different from that of normal seismic reflection lines because of the fixed receiver locations. With each OBS not being tied to the shooting ship, a wide range of offsets, from practically zero to the entire length of the line, can be achieved. This allows detection of near-vertical reflections as well as wide-angle reflections and refractions from deep layers. We deployed one OBS near each end of the line and one at about 20 km from each end. This assured a maximum source/receiver offset of at least 70 km for all OBS's.

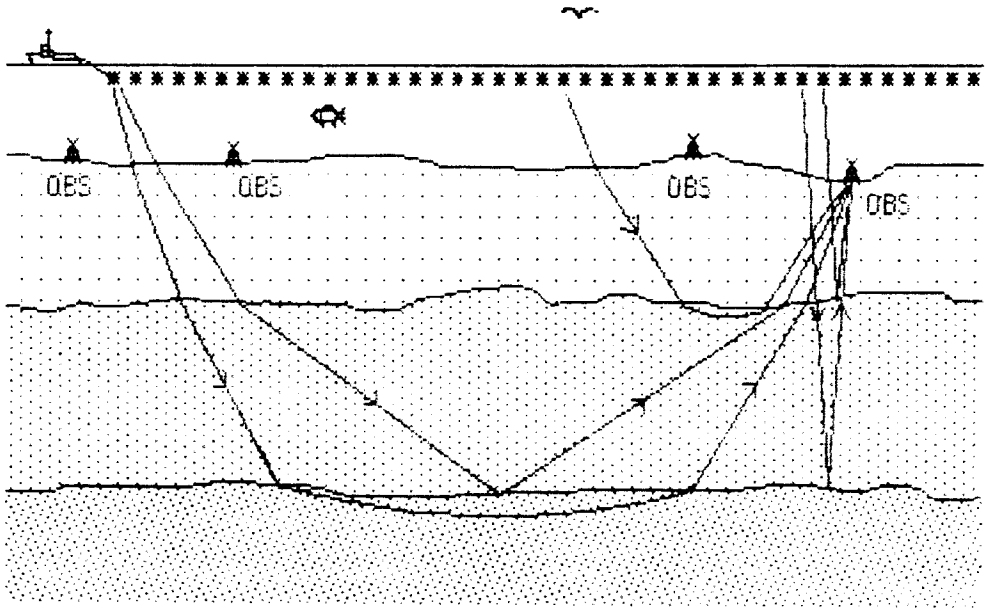

Fig. 2. Geometry of seismic line with four OBS's

Instrumentation

The ocean-bottom seismograph used for this experiment is a sophisticated seismograph package developed at the University of Texas for detection of seismic signals at the ocean floor. It is an integrated package consisting of the following components: a) a sensor system; b) a set of three preamplifiers; c) a set of three binary-gain-ranging amplifiers; d) a 3-channel signal multiplexer; e) a 12-bit analog-to-digital converter; f) up to 96K bytes of temporary data storage memory; g) a digital

Table 1. End coordinates of seismic lines

Line	Western End		Eastern End	
1	28°25.01' N	94°50.94' W	28°58.79' N	94°08.97' W
2	27°45.98' N	95°19.20' W	27°49.39' N	94°22.06' W
3	27°02.63' N	95°11.54' W	26°49.20' N	94°19.72' W
4	26°26.64' N	93°55.91' W	27°01.74' N	93°15.37' W
5	25°59.91' N	93°55.65' W	26°00.15' N	93°01.39' W

Table 2. OBS locations

Line	OBS	Latitude	Longitude	Depth, m
1	21	28°43.56' N	94°27.72' W	27
	22	28°47.59' N	94°22.60' W	27
	23	28°51.67' N	94°17.70' W	23
	31	28°33.67' N	94°40.35' W	32
	33	28°25.60' N	94°50.19' W	38
2	1	27°46.31' N	95°13.63' W	282
	3	27°48.66' N	94°37.05' W	366
	4	27°49.29' N	94°25.74' W	278
3	1	26°50.71' N	94°25.60' W	1317
	2	26°53.75' N	94°36.26' W	1529
	3	26°59.96' N	95°00.62' W	1441
	4	27°02.66' N	95°11.26' W	1362
4	1	26°57.31' N	93°20.48' W	1296
	2	26°50.56' N	93°28.73' W	1297
	4	26°28.09' N	93°55.03' W	1598
5	1	25°59.91' N	93°07.77' W	3150
	2	25°59.95' N	93°18.80' W	3138
	4	25°59.89' N	93°54.74' W	3151

cartridge tape recorder; h) a clock; i) an acoustic transponder; j) a release mechanism; and k) a set of recovery aids.

The sensor system is normally made up of one to three geophones, but may include a hydrophone. The binary gain ranging permits a wide dynamic range of over 96 dB. The temporary data storage memory, which is enough to store 48,000 12-bit data words, each with sign, exponent and component identification, is required because the tape recorder must be turned off during data acquisition to avoid vibration noise.

The data acquisition is controlled by three microprocessors for overall system control, clock control and tape recorder control. They are individually programmed to give wide flexibility in data acquisition mode (such as number of channels, sampling interval, record length and timing of recording), compensation of clock drift, formatting of data for recording, and release of the package from the ocean floor.

The electronics subsystems, geophones, the acoustic transponder and strobe lights to aid recovery are contained in a glass sphere, 17 inches (43 cm) in diameter, which fits snugly into a molded plastic cap. This buoyant package with two radio beacons and two orange flags to aid recovery constitute the recovery capsule, which returns from the ocean floor after data collection.

On deployment, the recovery capsule is attached firmly to a steel anchor frame by three stiff elastic straps linked by a stainless steel wire (Fig. 3). The frame has many spikes, which penetrate the ocean floor sediments to improve seismic coupling. The release of the package from the ocean floor for surface recovery is accomplished by electrolytically dissolving the stainless steel wire in sea water, triggered by one of three independent means: programmed release controlled by the main clock, preset release initiated by a backup clock, or acoustic recall by a surface ship.

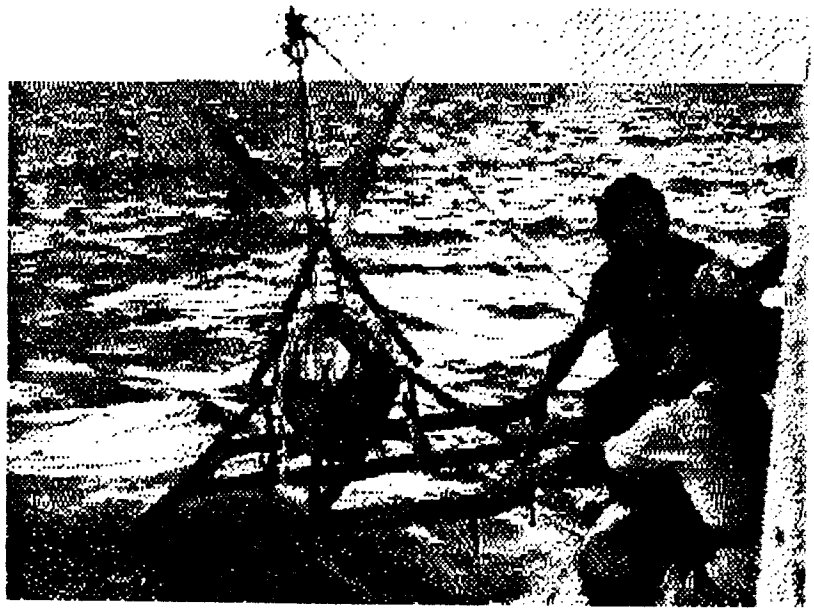

Fig. 3. The Texas OBS being deployed from R/V *Fred H. Moore*.

Field Parameters

Various parameters of the field experiment are listed below:

Source:	Two air guns, Bolt model 800C, 2000 in^3 (33 l) each, at 2000 psi (1.4×10^4 N/m^2)
Towing depth:	35 feet (11 m) [30 feet (9 m) for line 1]
Repetition rate:	30 sec
Ship speed:	5 knots [6 knots for most of line 1; 4 knots for lines 2-5 extensions; 3 knots for line 1 extension]
Shot spacing:	75 m [90 m for most of line 1; 60 m for lines 2-5 extensions; 45 m for line 1 extension]
Receivers:	4.5 Hz vertical geophone, Mark Product model L1BU [2.0 Hz vertical (Mark Product L22UD) and two 10 Hz horizontal (Mark Product L6A) geophones for line 1, OBS 21; 2.0 Hz vertical geophones for line 1, OBS 23] 600 m hydrophone streamer, 5 channels Sonobuoys
Passband:	4.5 - 20 Hz [30 Hz low pass for line 1]
Overall sensitivity:	9.0×10^{-10} (m/s)/DU [1.8×10^{-9} for 2 Hz geophone and 1.6×10^{-9} for 10 Hz geophone]
Recording window:	20.4 s, sliding [15.0 s for line 1, OBS 21-23]
Sampling interval:	10.008 ms [7.334 ms for line 1, OBS 21-23]

Navigation

We used Loran-C as the primary means of navigation to locate each OBS and shot point, supplemented by satellite navigation for absolute reference. The procedure was to use geographic coordinates as determined by satellite navigation to estimate the additional secondary correction factor (ASF) needed for computation of latitude and longitude from the observed Loran-C time difference (TD) values. The ASF values thus determined and used for the computation are listed in Table 3.

Table 3. Loran-C additional secondary correction factors

Line	WASF,μs	XASF,μs
1	1.5*	1.2*
2	1.1 ± 0.1	1.5 ± 0.6
3	0.4 ± 0.2	0.0 ± 2.0
4	0.4 ± 0.3	0.9 ± 1.6
5	0.3 ± 0.4	1.1 ± 2.2

*The ASF values used for Line 1 are not based on satellite navigation, but are based on data on Loran-C tables and nautical charts.

When individual TD readings are used independently for each shot, however, their precision is not sufficient to allow computation of the relative locations of shot points at high accuracy. Therefore, we first smoothed the entire set of measured TD values for each line using piecewise-continuous, cubic Hermite functions, and then computed more accurate estimates of TD values at each shot from the smoothed TD functions. Finally, we computed shot coordinates using these accurate TD estimates. We estimate the relative distance between shots to be accurate to better than 1%. However, absolute locations may be off by as much as a mile.

Field Experiment

The experiment was conducted from the R/V *Fred H. Moore*, on cruises Nos. FM-17 (June 8-9, 1983; Test Cruise 2 covering a part of Line 1), FM-19 (August 24-25, 1983; Test Cruise 3 covering the remainder of Line 1), and FM-20-02 (November 27-December 4, 1983; Lines 2-5). The primary purpose of the first two cruises was to test the OBS's newly configured and programmed to acquire signals from air-gun sources. The last cruise exactly retraced the four ESP (expanding spread profiling) lines shot earlier in the month from R/V *Fred H. Moore* and R/V *Gyre*.

On each line, OBS's were deployed at predetermined locations. The line was then retraced while shooting the air guns at 30 second repetition rate. On Lines 2-5 we pulled a short streamer, collecting supplementary reflection data. Finally, the line was retraced for the third time to recover the OBS's.

A total of 22 OBS's were deployed during the experiment and 18 of them were recovered containing data (Table 2). The other four were recovered but the recording system had failed. In no case did more than one instrument fail on a line, and all the failures were on instruments near the center of the line, not the more important instruments at the ends of the lines.

DATA PROCESSING

Standard processing of the acquired data consisted of the following steps:

a) Reformatting of the seismic data on cartridge tapes to SEG-Y format: The original OBS data were written on each cartridge tape in a special packed format to conserve tape usage. The data were reformatted to standard SEG-Y format and were rewritten onto a standard computer tape.

b) Post-cruise recomputation of shot locations: Shot locations were recomputed from the measured Loran-C TD values using the ASF values estimated from comparison with the satellite navigation coordinates as described above.

c) Location of OBS based on water-wave arrival times: The actual location of each OBS was slightly different from its deployment and recovery locations because of the drift due to current and wind. The observed water-wave arrival times were used to determine the actual location of each OBS as well as the exact clock correction, at the time of the passage of the shooting ship over the instrument, using a least-squares inversion of the arrival times.

d) Merging of navigation data into SEG-Y format tapes: Revised navigation data based on the recomputed shot and OBS locations and clock drift were merged into the initial SEG-Y format tapes described above.

e) Stacking of traces into uniform offset bins: The acquired seismic traces were not evenly spaced in offset because the ship speed varied from time to time while the shooting was done according to a preset time schedule. To facilitate interpretation of record sections, we 'stacked' the traces into 100 m bins using a stacking velocity of 6 km/s. The offset range for this stacking was short enough (about ±50 m) so that attenuation of arrivals of phase velocities different from 6 km/s was negligible. Most bins contained 1 or 2 traces.

f) Plotting of record sections: The binned traces were plotted to produce the basic seismic record section plots.

g) Deconvolution: Since the air guns used for this experiment were not tuned, several cycles of bubble pulses appeared following each arrival. Though these regular cyclic arrivals are quite advantageous for recognition of weak refraction arrivals at far distances, they interfere with identification of reflected arrivals at near ranges. In order to reduce the bubble pulses, we applied deconvolution to the near-offset (up to about 25 km) data to be used for reflection moveout analysis. Deconvolution filters based on either the bubbled water-wave arrivals or the entire trace were used with satisfactory results.

h) Slant stack to tau-p domain: When conditions are favorable, i.e., the layers are nearly flat and laterally homogeneous, the data in the time-distance domain can be transformed into the tau-p (intercept time - ray parameter) domain by slant stacking [*Stoffa et al*, 1981].

The processed products d) through h) were then used for further processing and interpretations. Figures 4a through 4e (on fold-out pages) show reduced copies of seismic record sections. The multichannel data shown on record sections of Lines 2-5 are from our short streamer. They are also stacked into 100 m bins and are displayed in

a filtered and deconvolved single-fold section. Figures 5 and 6 show reduced samples of deconvolved and slant stacked record sections, respectively.

The following figures are on the fold-out pages.

Fig. 4a. Line 1 seismic record sections.

Fig. 4b. Line 2 seismic record sections.

Fig. 4c. Line 3 seismic record sections.

Fig. 4d. Line 4 seismic record sections.

Fig. 4e. Line 5 seismic record sections.

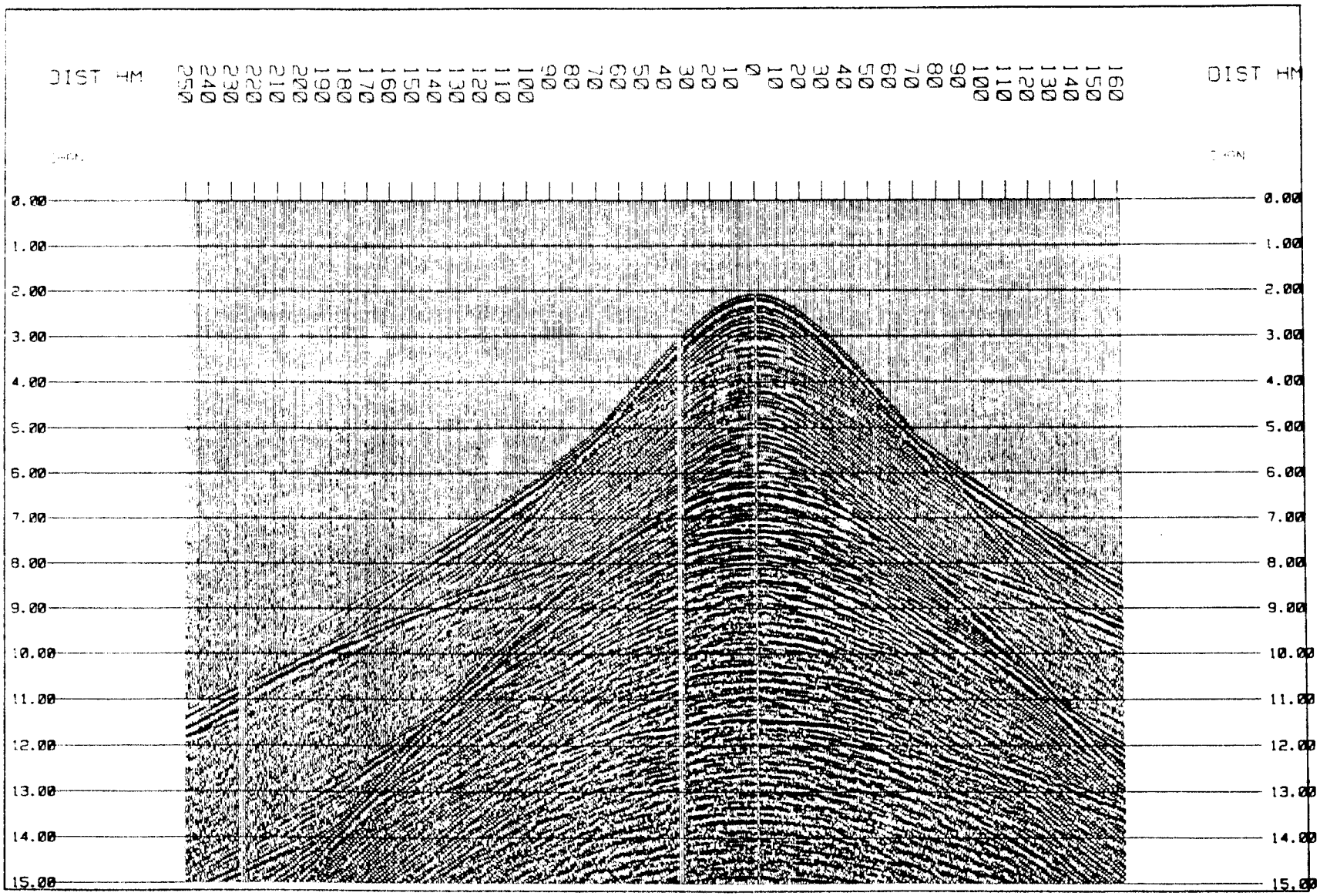

Fig. 5. Deconvolved partial record section for Line 5, OBS 2. Distances are given in units of 100 m and times are in sec.

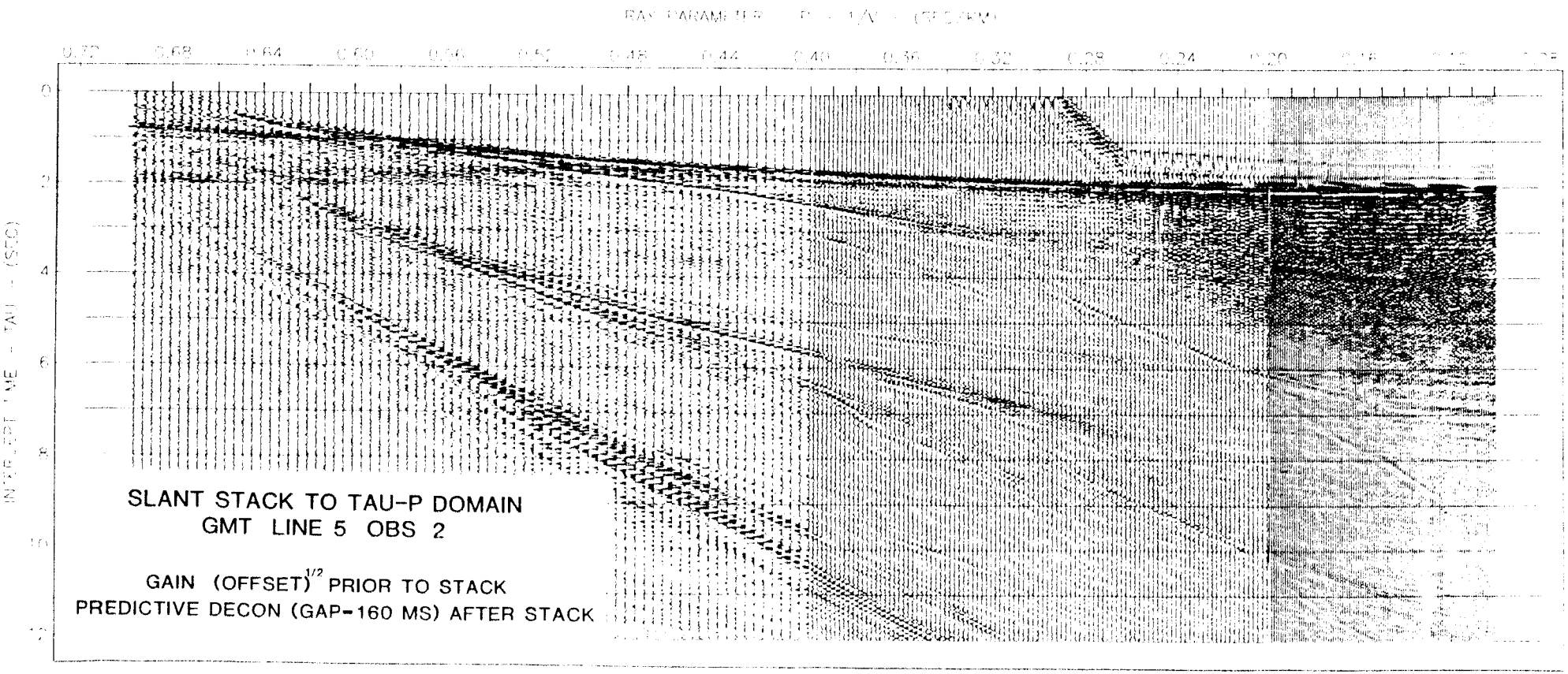

Fig. 6. Slant stacked record section for Line 5, OBS 2 in the tau-p domain.

ANALYSIS AND INTERPRETATION

Analysis Methods

There are several methods available in analyzing and interpreting the kind of seismic data acquired in this experiment. The simplest and most common method for interpreting large offset refraction data is in terms of flat, constant-velocity layers as calculated from the slopes and intercept times of refracted arrivals. If the structure is not too complicated, this method will give a rough estimate of the velocity-depth profile. The method, however, breaks down if there are velocity inversions or if large lateral velocity variations exist.

As in ordinary reflection work, near-vertical reflection data can be analyzed using moveout of arrivals with offset. The larger offsets in this experiment allow us to determine interval velocities more accurately at greater depths, although the large offsets require us to account for non-hyperbolic moveout.

Since the data acquired in this experiment are of high spatial density and since they cover a wide offset range including both pre-critical and post-critical reflections, they can be slant stacked successfully into the tau-p (intercept time vs. ray parameter) domain. The transformed data can be inverted to obtain bounds on the velocity-depth function.

These procedures, however, assume either that the structure is horizontally homogeneous or that lateral variation is at most gradual. Unfortunately, neither assumption is valid for some of the areas covered in the present experiment since parts of several of the lines of the experiment lie over shallow salt structures which exhibit a high degree of lateral heterogeneity. The results obtained by assuming one dimensionality give only very approximate solutions for these lines.

The method we have found most successful is a combination of various one-dimensional (1-D) techniques with two-dimensional (2-D) ray tracing. Also essential in this analysis are multichannel reflection data. The procedure we followed can be summarized as follows:

a) First, we pursued one-dimensional analyses as far as the data allow. This included conventional layered-model interpretation of refraction arrivals, applicable for both shallow and deep structures; moveout analysis of pre-critical reflection data for interval velocities, generally useful down to about 10 km depth; and if conditions were favorable, such as on Line 5 and parts of lines 1, 2 and 3, inversion of tau-p slant stacked data for velocity bounds [*Garmany*, 1979; *Garmany et al.*, 1979; *Diebold and Stoffa*, 1981].

b) On a multichannel reflection record section, we identified major reflecting interfaces and measure two-way vertical travel times to these interfaces at key locations. Then using the velocities as determined in step a) above, we converted the time section into a depth section. This gave the initial two-dimensional model for the shallow structure near each OBS.

c) We examined the OBS record section and identified any unusual arrivals, such as reflections from the top of a salt intrusion and refractions through the salt (Fig. 7), and then used this information to further refine the initial 2-D model of step b) above.

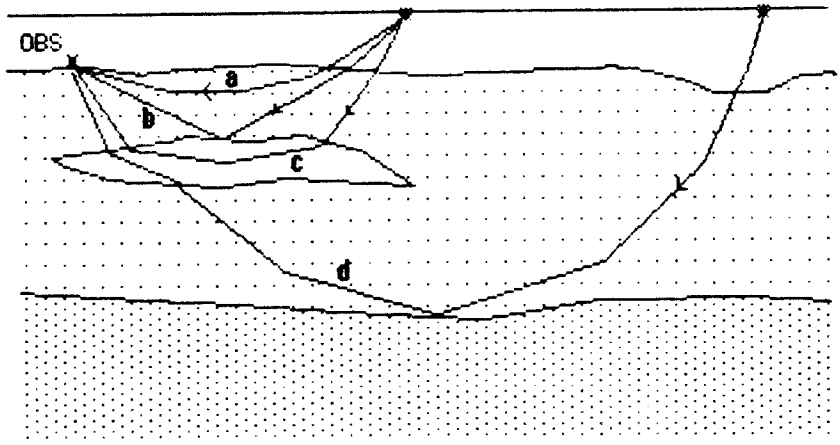

Fig. 7. Seismic rays commonly observed in areas with allochthonous salt: a) refractions and reflections from shallow sedimentary layers; b) reflections from top of salt; c) refractions through upper part of salt; d) refractions and reflections from deeper layers through salt.

d) Using this as a starting model, we shot a set of rays in reverse, originating at each OBS location and ending at shot points near the sea surface, and computed distance and travel time for each ray. We then compared the computed travel times with observed travel times, adjusted the model accordingly and repeated the procedure until a satisfactory fit was obtained. We also paid attention to any focusing and defocusing of rays, which should be manifested in the observed amplitudes.

e) Once a satisfactory near-OBS shallow structure was constructed, we added deeper layers based on the information gained in the first step to make a model for the entire line. Then, we shot another set of rays that penetrated through the shallow structure and appeared at large offsets. Finally, we compared them with observations and adjusted the structural parameters to arrive at an acceptable model of the deeper structures.

Line interpretations

Line 5 (*cf.* Fig. 4e)

Line 5 is located in the central Gulf of Mexico just south of the Sigsbee Escarpment on the western Gulf rise. The multichannel reflection data show that the sedimentary column is made up of nearly horizontal layers. The OBS records show first arrivals of smoothly varying slope between offsets of 6 and 25 km, indicating continuously increasing velocity with depth in the shallow sedimentary column. Between offsets of 25 and 35 km there is a low amplitude refraction arrival from what are interpreted to be carbonate rocks overlying basement. This arrival is followed by a high amplitude basement refraction in the 30 to 42 km offset range. The refraction from the upper mantle is clearly observed out to distances of about 61 km at OBS 2 (the limit of the data) and 70 km at OBS 4.

Reflection as well as refraction arrivals are observed on the OBS records from this line. Many of these arrivals are clearly visible on deconvolved record sections, e.g., Fig. 5. Moveout analysis of the reflected arrivals gives us another means of estimating a one-dimensional velocity profile under each OBS. Since these reflections cover much wider offset ranges than usual on multichannel reflection data, the estimated velocity values are more accurate than those from multichannel data at great depth. We must, however, use non-hyperbolic functions for the analysis.

The most prominent reflection is observed at about 7 sec at zero offset on all three OBS's on this line and corresponds to the middle Cretaceous unconformity (MCU), an erosional surface representing the top of the Challenger unit, prominent on reflection profiles throughout the deep Gulf of Mexico and has been considered to correspond to a major increase in refraction velocity. *Buffler* [1984] suggests that this prominent increase in velocity probably represents a major lithologic change from deep water clastics above to predominantly deep-water carbonates below. This arrival is not only strong at close ranges but also can be traced to very long offsets. The high amplitudes observed between distances of 20 and 27 km suggest that the critical distance for this arrival lies in this offset range.

The highly consistent air-gun source yields data in which details of the signal near the critical distance can be observed. The low-amplitude carbonate refraction breaks out from the high amplitude MCU reflection at an offset of about 28.5 km (arrival time - 12.2 sec) on OBS 1 and 2 records. The crustal refraction breaks out at about 28 km (arrival time - 12.5 sec) from the large-amplitude, wide-angle reflections of both the MCU and the bottom of the Challenger unit. This refraction grades from relatively low amplitude to large amplitude between 34 and 42 km. This characterizes the variation in the velocity gradient within the Challenger unit. Although one cannot unambiguously trace the Moho reflection, the mantle refraction is observed to cross over from the crustal refraction at the offset close to 45 km. The large amplitude of the crustal refraction could also be a result of the constructive interference between it and the mantle refraction arrivals.

The high-density data of this experiment also allow us to use the inversion technique based on tau-p slant stack of the data for these nearly horizontal strata. As described in more detail later, the inversion results show velocity profiles consistent with the other 1-D results under all three OBS's, with major changes in velocity gradient at 5, 10 and 15 km depths, corresponding to the top of the consolidated sediment, the MCU and the top of the crystalline basement, respectively.

We completed the analysis for this line with 2-D ray tracing, using a combined result of the above 1-D analyses as a starting model. As expected for this relatively simple line, the final result, Fig. 8, is generally consistent with the various 1-D results. In addition, it shows the depth to the Moho to be about 20 km at the western end of the line with a slight dip towards east reaching to 21 km at the eastern end of the line.

Line 4 (*cf.* Fig. 4d)

Line 4 is 93 km long and trends NE-SW just north of the Sigsbee Escarpment (Fig. 1). This location is characterized by thin, low-velocity sediment atop unusually shallow, high-velocity salt structures. The large velocity contrast between the salt and the sedimentary cover and the intense deformation of the salt surface contrast sharply to the nearly uniform structure we considered along Line 5 and limit the methods of interpretation we can use. Although we used 1-D methods to develop a starting model,

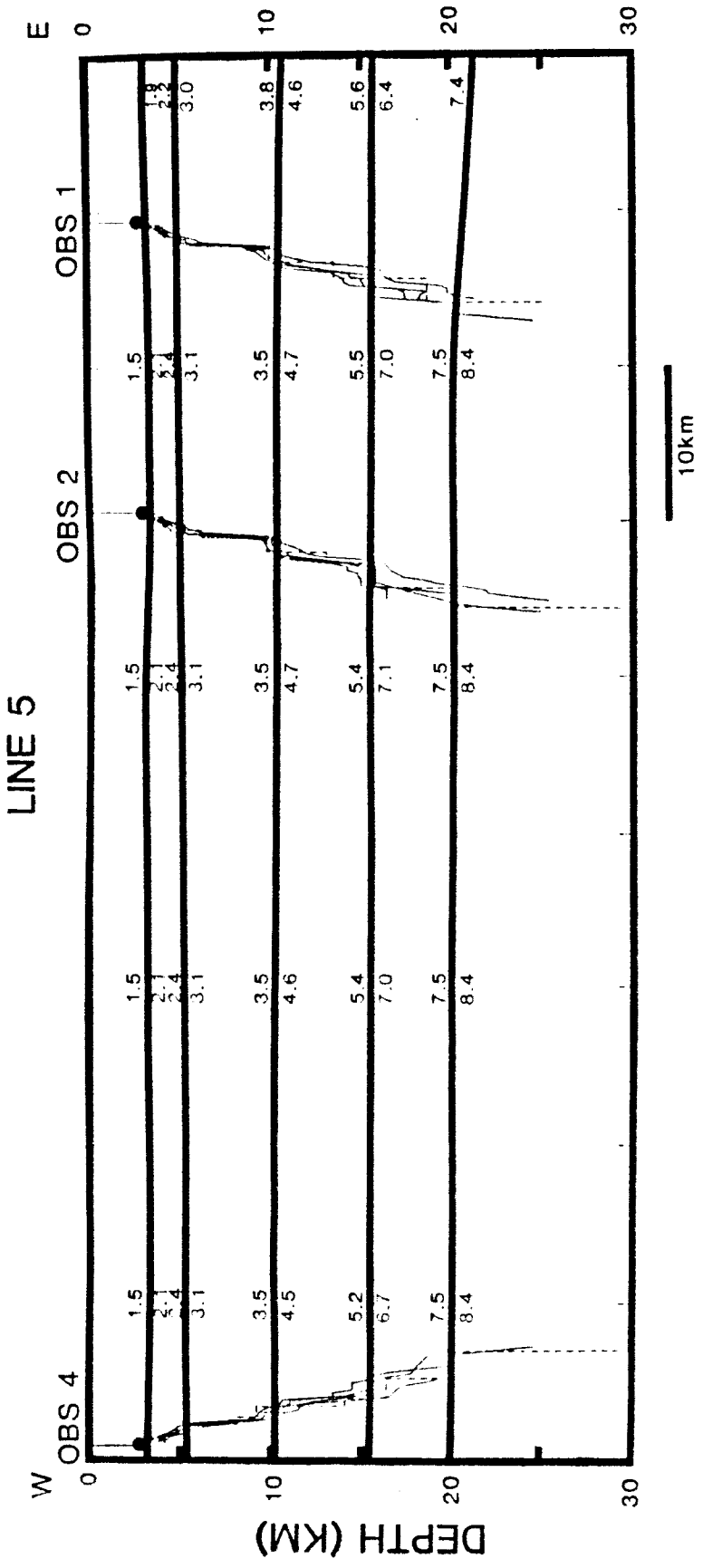

Fig. 8. Line 5 structural profile.

only the 2-D ray tracing technique was suitable for determining the velocity-depth structure under this line.

The high amplitude reflection from the top of the salt is prominent in the reflection section (top record section of Fig. 4d). The arrivals of high amplitude and high apparent velocity, shallow in the OBS sections (remainder of Fig. 4d), are refracted arrivals through the salt. These salt refractions stop abruptly at a certain distance which differs from one OBS to another. Immediately behind this salt arrival is a large gap in arrival time, which we interpret to signify the presence of a low velocity zone below the high velocity salt. As will be discussed in more detail later, this characteristic feature of the salt arrivals as observed on each OBS gives us the basic data to estimate the thickness of the salt as well as the velocity structure below the salt.

The shallow, high-velocity salt severely disrupts arrivals from below, so the deeper structures can be reliably mapped and interpreted only after the structure of the salt and the overlying sediment is determined. Thus we have used 2-D ray tracing to model the reflection and refraction arrivals working from the top of the model downward. The resulting structure, Fig. 9, has the following main features:

1. A low-velocity sedimentary layer, interpreted to be of Tertiary age, with velocities ranging from 1.90 km/s just below the sea floor to about 2.5 km/s at an average depth of 2.5 km. The relatively high velocity at the base of the sediment may be due to overcompaction similar to that encountered at DSDP Hole 92 [*Worzel and Bryant*, 1973] in a similar geologic setting. *Buffler et al.* [1978] suggest that tectonic forces that are related to the thrusting of the salt tongues could cause compaction of overlying sediments. The thickness of this layer is mainly controlled by the highly deformed surface of the salt below it.

2. A continuous salt body, 1.5-2.5 km thick, underneath the sediment. The velocity of the salt varies from about 4.1 km/s at the top to about 4.6 km/s at the bottom. Since the velocity of pure salt is approximately 4.6 km/sec [*Papadakes*, 1963], the lower velocity associated with this salt indicates that the tongues may consist of salt mixed with low velocity sediment. *Buffler et al.* [1978] found interval velocities ranging from 3.9 to 5.2 km/s for this type of structure while processing multichannel data from the lower slope of the Gulf. This line is located near the basinward end of the salt, most probably a Mesozoic deposit that since has moved southwards and upwards to form a continuous allochthonous salt front along the lower slope of the western Gulf. The highly rugged surface of the salt may have been caused by sediment scouring and salt dissolution during the salt movement.

3. A thick, sedimentary layer with its velocity varying from 3.85 km/s at 4 km depth to 4.5 km/s at 11 km depth. The velocity range suggests that this layer consists mainly of clastics mixed with significant amount of salt. The bottom boundary of the layer is a highly reflective surface that is interpreted to be the MCU.

4. A layer below the MCU with laterally varying velocities. The velocity varies from 5.5-7.4 km/s at the southwestern end of the profile to 5.0-6.3 km/s at the northeast. These high velocities are typical of carbonates. Although we did not observe any crustal arrivals below the salt, these high carbonate velocities may suggest that the basement is relatively shallow under the allochthonous salt.

We were unable to observe any crustal arrivals under this line. This may be due to large attenuation of seismic energy caused by reflection and possibly by mode conversion, one at the sediment/salt interface and another at the MCU.

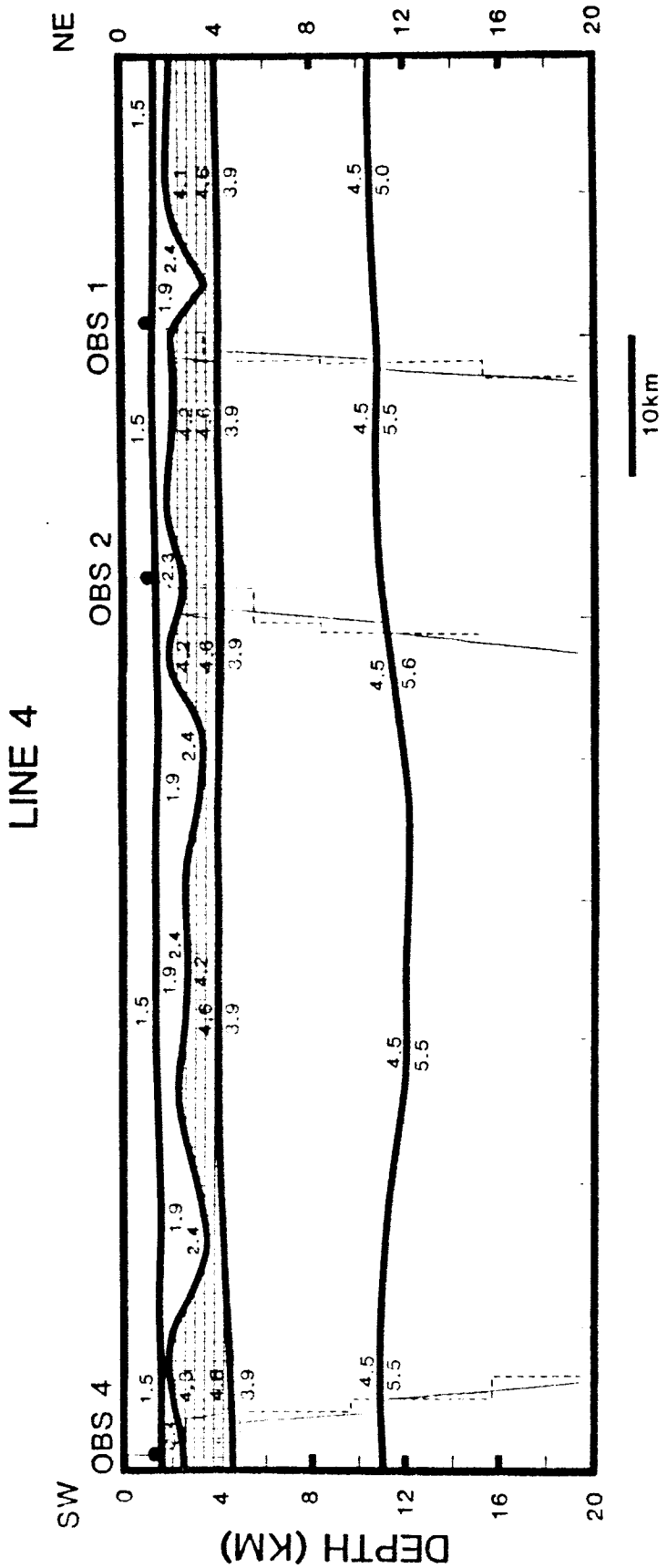

Fig. 9. Line 4 structural profile.

Line 3 (*cf.* Fig. 4c)

This line is 90 km long and trends ESE-WNW in the middle continental slope north of the Alaminos Canyon (Fig. 1). It is located in a thick sedimentary basin, with observable salt structures near the eastern end and possibly at the western end of the line. The reflection section (Fig. 4c, top panel) shows the shallow sedimentary section dipping slightly towards a salt dome to the east. The refractions through the salt, observed with high apparent velocity, are clearly visible on the record sections of OBS's 1 and 2. To the west of OBS 1, the record section shows a characteristic low-velocity zone under the salt: there is a delay of about 2 sec after the salt refraction before the arrivals from below the salt are observed. High-velocity, lower-crustal arrivals are observed on all OBS record sections except OBS 1.

Conventional refraction data interpretation shows a relatively thick, low-velocity, shallow sedimentary section reaching to about 10 km depth. The 3.0 km/s velocity observed at this depth may represent overpressured shale which is prevalent in the Texas/Louisiana slope. Moveout analyses of deconvolved OBS record sections are also quite useful for OBS's 2 and 3. However, no identifiable reflections could be observed at OBS 4, and only very few reflectors are apparent at OBS 1 mainly because of the presence of salt.

Transformation of the data at OBS's 2 and 3 into the tau-p domain and the subsequent inversion by both extremal and tau-sum methods confirm that the sedimentary section consists of a nearly homogeneous layer down to a depth of about 10 km. An apparent change in velocity gradient between 12 and 16 km under OBS 3 corresponds to the crustal arrivals which are observed on all the record sections.

The result of 2-D ray tracing for the entire line, Fig 10, is generally consistent with the above 1-D results under OBS's 2 and 3. In addition, it shows a 2.5 km thick salt section starting at about 2.5 km depth near the eastern end of the line. The salt velocity ranges from about 3.8-4.0 km/s to 3.1-3.4 km/s along the section. The decrease in velocity may be due to a thick shale sheath dragged along with the salt from its original depth of deposition, or it may be due to very dirty salt. The salt is underlain by nearly homogeneous low-velocity sediment with a velocity of about 3.0 km/s. This section extends down to the MCU. The Challenger unit averages about 4 km in thickness. The most interesting feature of this velocity section is the observation of a thin crust which may be interpreted to be either oceanic or highly attenuated continental crust. This crust measures about 7 km thick to the west and thickens to about 9 km to the east. The mantle arrivals recorded at all but the easternmost OBS put the Moho at very shallow depths of between 18 and 20 km to the west and 23 km to the east.

Line 2 (*cf.* Fig. 4b)

This line is located on the upper slope and trends approximately E-W, parallel to and just outside the 100-fathom bathymetric contour. Unlike the lines farther to the south on the middle and lower slope, this line shows little or no observable shallow salt structure. Deep-seated salt may be present (Fig. 4b, top panel). Deep salt masses, however, cannot be identified by velocity alone using the OBS records since the sediments at large depths have velocities comparable to that of salt. The record section west of OBS 3 shows a large-amplitude arrival with relatively high apparent velocity breaking out from the linear sedimentary arrivals at about 10 sec of travel time. These deep first arrivals may suggest the presence of deep salt with some structure.

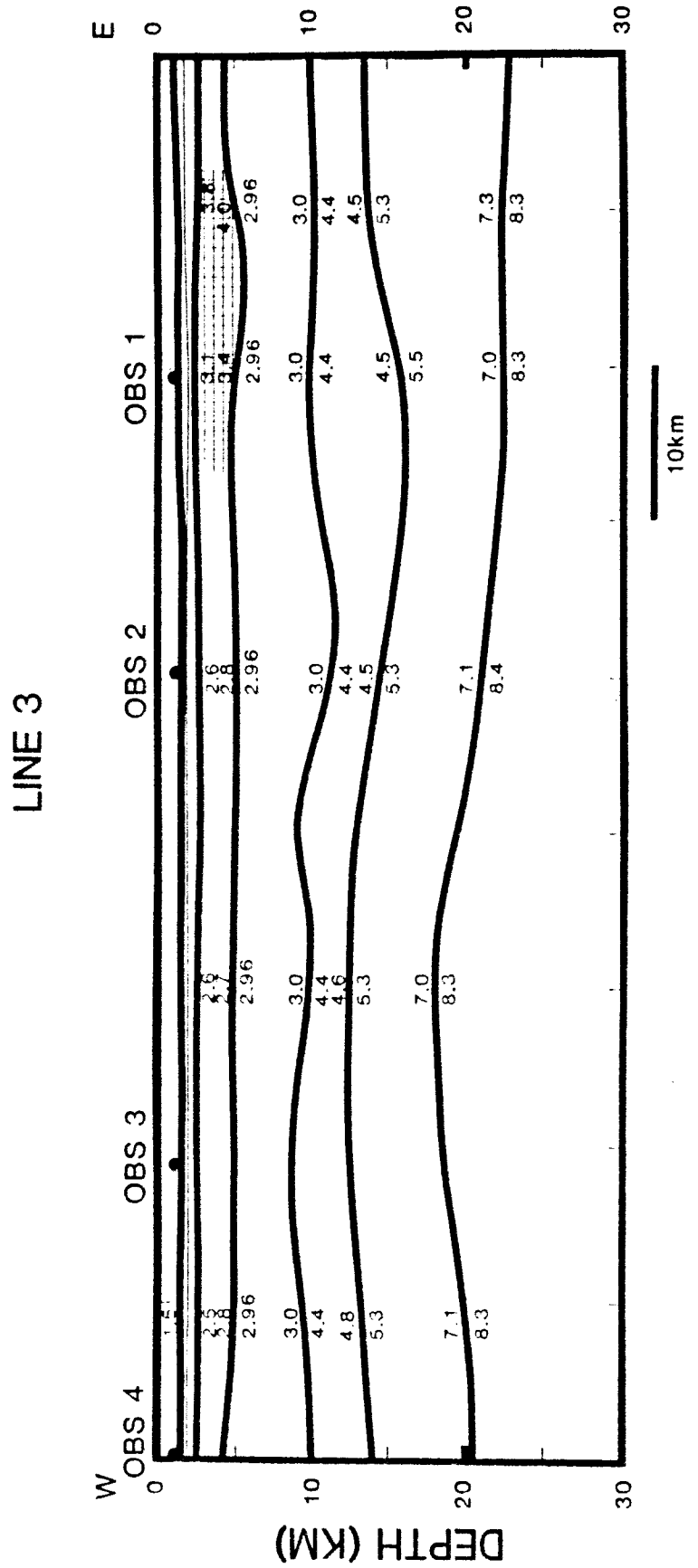

Fig. 10. Line 3 structural profile.

Additionally, some intermittent high-amplitude arrivals from great depths are also observed on the OBS record sections, suggesting the existence of large-scale lateral heterogeneity deep in the section. A broad, dome-like structure is observed centered at about 64 km from the western end of the line. Other structures can be seen at about 29 km and also at the eastern end of the line.

The conventional 1-D inversion of refraction arrivals indicates the presence of a strong refractor with apparent velocity in the 4.9-5.5 km/s range at a depth of 9-10 km at all three OBS's. Deeper arrivals are observed only at those OBS's which were favorably located. They include a 6.5 km/s layer at a depth of 21.5 km at OBS 3 and an 8.3 km/s layer at a depth of 25 km to the west of OBS 1. Both the quoted velocities and depths are apparent because of the 1-D analyses.

We have performed moveout analyses of deconvolved record sections from OBS's 3 and 4. Although the data can be fit, there exists sufficient lateral heterogeneity, manifested by the asymmetry of the arrivals, to doubt the appropriateness of this analysis.

We have also transformed the data from OBS's 1 and 3 into the tau-p domain and inverted them using the extremal and tau-sum methods. The large velocity increase at a depth of about 10 km as indicated by the conventional refraction analysis is also seen on these inversion results. The inversion of OBS 3 data shows a sudden increase in velocity at a depth of about 15-17 km. However, the two inversion methods estimate its depth differently, indicating that the structure under this line is not likely to be 1-D.

Using the 1-D analyses, we built a starting model for 2-D ray tracing. We obtained a 2-D structure for the line which matched the observed OBS data. These results, Fig. 11, show that the top of the 4.9-5.3 km/s layer is located at 11.6 km under OBS's 1 and 3. The large amplitude arrivals from this layer, observed at 32-43 km offsets on the records of OBS 1 and at 33-53 km offsets on OBS 3, turned out to be the results of the strong velocity gradient in the layer between OBS 1 and OBS 3. At OBS 4, the top of this layer is deeper at 12.4 km.

There is some lateral variation in velocity along the line. The presence or absence of salt structures at depths cannot be easily established by velocity alone, but it is apparent that there may be some salt deposits at depths below 7 km. The seismic boundaries are more planar below 10 km depth. There is a thickening of the 4.9-5.6 km/s layer towards the west. Although the conventional refraction inversion places the Moho (8.3 km/s velocity) at a depth of about 25 km under OBS 1, the more realistic 2-D inversion indicates that it is probably deeper than 25 km. The shallower depth calculated from the conventional analysis may be due to the effect of the minor shallow distortions between OBS 3 and OBS 4 locations, which reduce the observed intercept times. Thus, the crust is thicker under this line than under Line 3, with the Moho deeper than 25 km.

LINE 1 (*cf.* Fig. 4a)

Line 1 is a 93 km line trending NE-SW on the continental shelf in water depths that vary from 26 m at its northeastern end to 40 m at its southwestern end. The line is located along the gravity high which parallels the coast. Although we acquired no reflection data simultaneously with the OBS data, the apparent travel times of arrivals as seen on the OBS record sections show that the sedimentary column underneath the

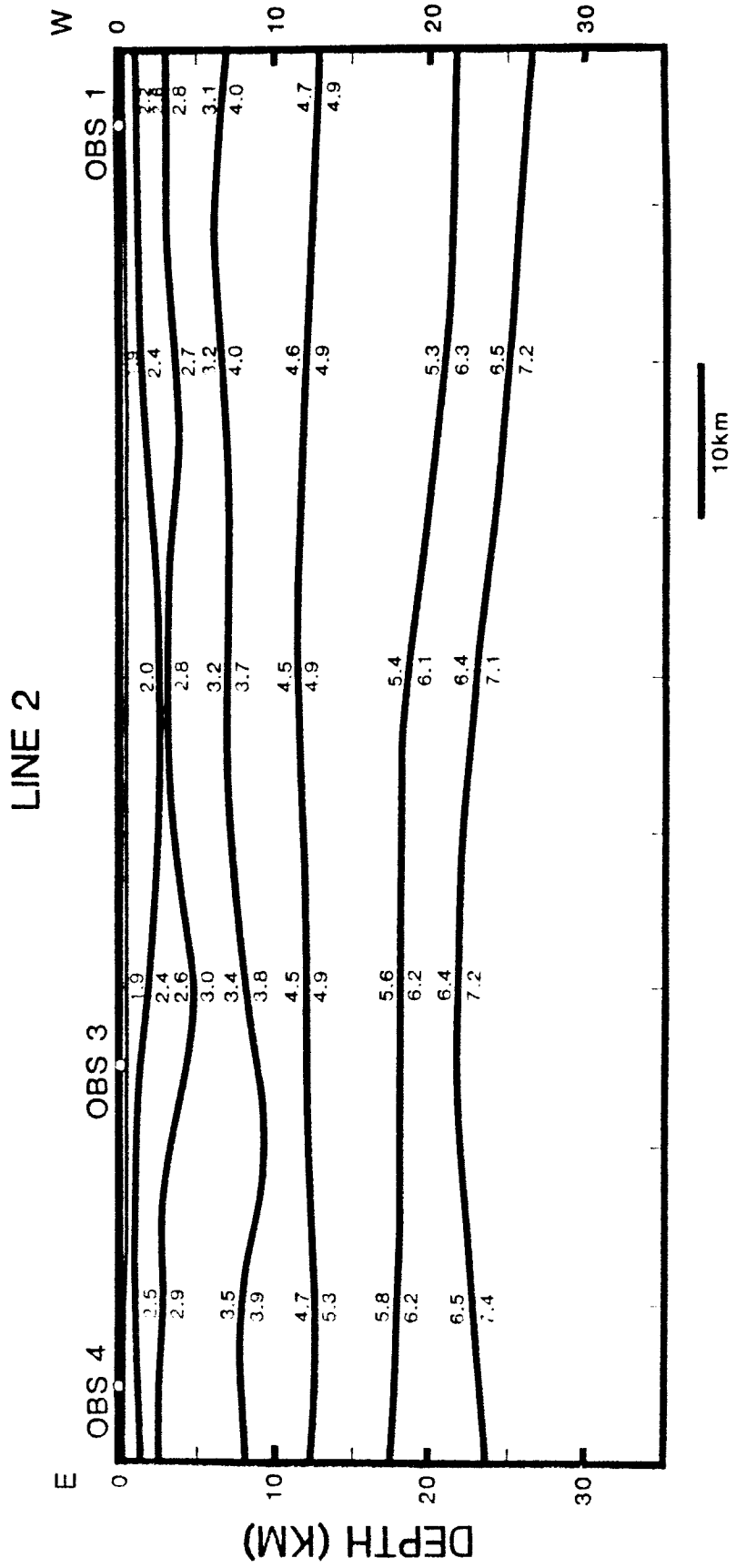

Fig. 11. Line 2 structural profile.

line has a nearly horizontal structure except at the extreme southwestern end of the line, where there exists a salt dome. Because of the simple structure, we analyzed these data using only 1-D techniques.

The result, Fig. 12, shows a smoothly increasing velocity in the sediment down to about 8 km depth. A highly reflective interface, which we interpret to be the MCU, is observed at a depth of 8-8.5 km, below which the velocity increases to 4.1-4.2 km/s. This interface is not identified further west at OBS 33 site, probably because of the shallow salt there. Carbonate and salt may have nearly the same seismic velocity, and thus cannot be distinguished by velocity alone. A 5.9 km/s layer observed at about 15 km depth represents the top of the crust. The fastest arrival we observed along this line is the 7.2 km/s lower crustal arrival in the eastern half of the line from a depth of about 21 km. No faster arrivals were observed, implying that the Moho under this line is deeper than 25 km, confirming that the crust thickens northwards towards the continental United States.

Regional Interpretation and Discussion

We obtained a total of eighteen OBS seismic record sections from five lines in an area extending from the Texas continental shelf to the continental rise of the western Gulf of Mexico. This is an area where earlier efforts to delineate the deep structure by conventional reflection and refraction surveys have been hampered by the existence of thick sediments and especially of numerous salt intrusions that cover much of the slope area. In the present study, we have improved these survey methods through the use of OBS's and air guns, extending the offset ranges for pre-critical and post-critical reflections, greatly increasing the spatial density for refraction observations at far distances, and combining interpretation of both reflection and refraction arrivals using modern techniques of data processing and analysis. The results have been presented line by line above. In this section we combine these results and attempt a regional synthesis.

The structural trend in the area roughly parallels the coast line. Therefore, we projected the velocity profile at each OBS location as derived in the above line-by-line interpretations onto a NNW-SSE line (A-A' of Fig. 1) roughly perpendicular to the coast line. On this projection, we also attempted to correlate major identified layer boundaries, Fig. 13.

A thick sedimentary sequence covers the entire study area. The thickness of sediments does not change appreciably across the profile: about 13 km both under the continental shelf and the rise, but increasing to about 15 km in places under the slope. In the upper slope region, the sedimentary column contains thick, relatively low-velocity material (velocity = 3.0 km/s) down to a depth of approximately 10 km, which we interpret to be mostly overpressured shale. Further south under the mid to outer slope, this sediment is severely disturbed by the presence of salt bodies.

The salt bodies are the most noticeable features under the continental slope of the northwestern Gulf. They are observed under all three lines located on the slope. In the upper slope region, most of the salt features appear to be deeply buried, with diapirs of limited lateral extent reaching to a depth of a few hundred meters below the sea floor. In the middle and outer slope regions, massive salt bodies generally become shallower, but at the same time thin towards the south with an average thickness of about 2.5 km under Line 4. We interpret the presence of low-velocity clastic sediments below these allochthonous salt bodies. The northward extent of these salt bodies is not clearly

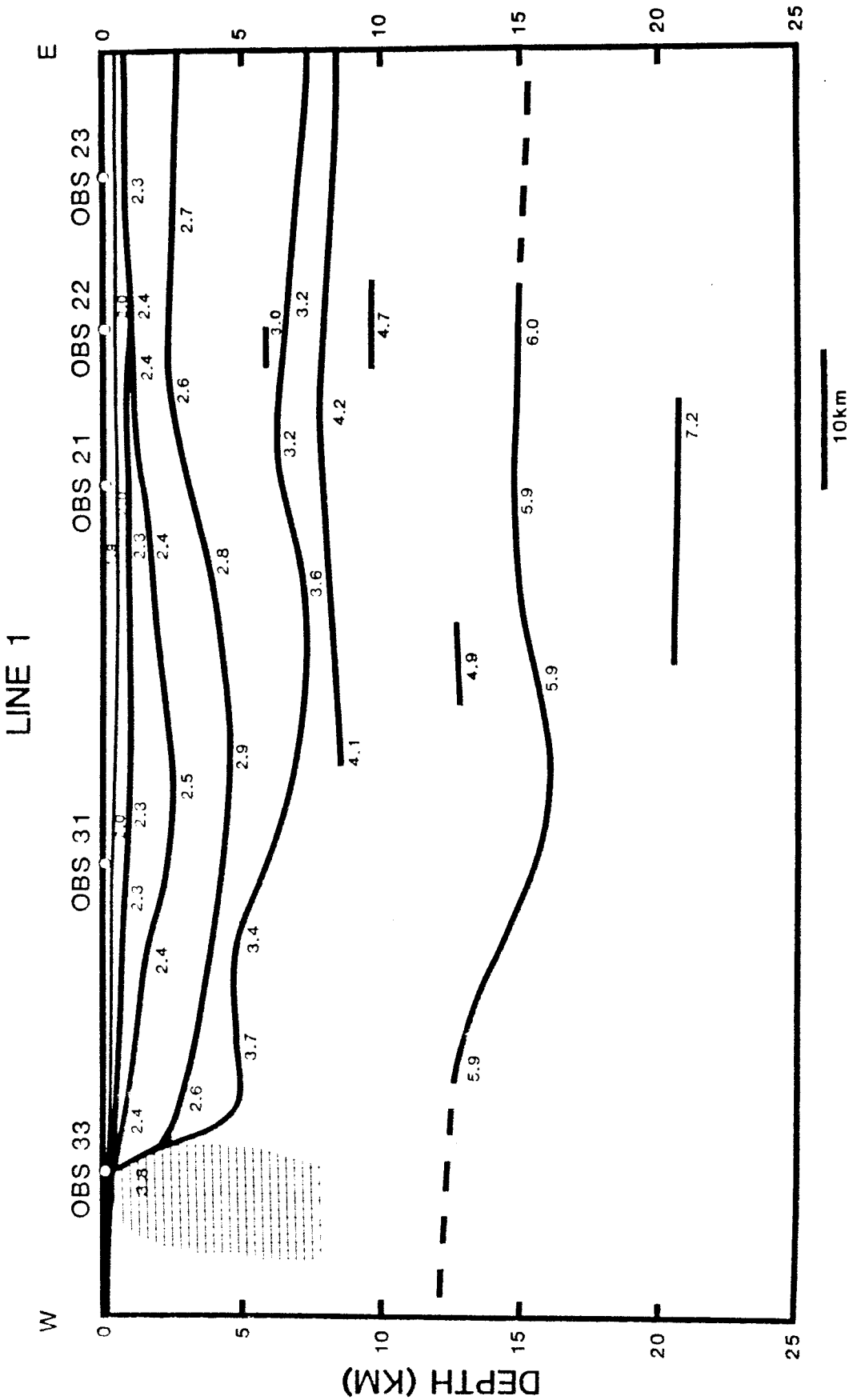

Fig. 12. Line 1 structural profile.

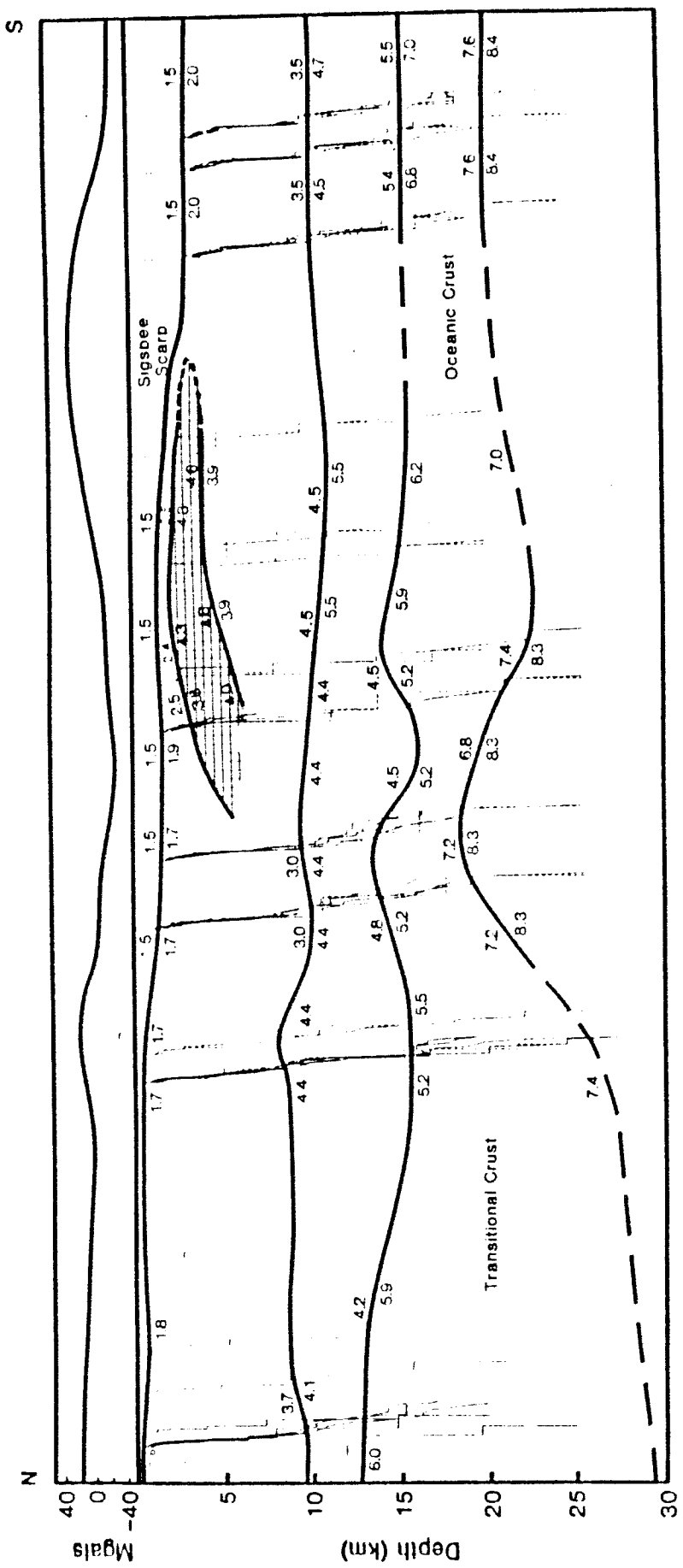

Fig. 13. Structural cross section projected onto line A-A' of Fig. 1. The top section shows free-air gravity anomaly interpolated from the data of USNS Keathley cruises in 1968-1970 compiled by *Pilger and Augelich* [1984].

defined by this experiment because salt becomes seismically indistinguishable from surrounding sediments at depth. However, the low gravity anomaly on the mid slope, Fig. 13, may suggest this to be the major source region of the allochthonous salt observed in the outer slope.

The MCU is generally quite clear on multichannel record sections from the deep Gulf basin, but loses its character and becomes difficult to identify below the continental slope mainly because of the interfering salt structures above. With the present experiment with OBS and air guns, we could follow this prominent reflector most of the time under the slope using wide-angle reflections from this interface characteristically observed at offsets greater than 10 km. The discontinuity, which is observed at a depth of about 11 km on the continental rise, shows a gentle rise in section under the slope, shallowing to about 9 km under the shelf just south of Galveston. The relatively high velocity of the sediment between the MCU and the allochthonous salt of outer slope may be due to the presence of additional patches of salt in this sedimentary column. The layer below the MCU, believed to be carbonate, generally has a velocity of 4.5 km/s at the top and increases with depth towards the basement. The velocity again is exceptionally high under the outer slope. This may suggest shallowing of basement.

The interface we interpret to be the crystalline basement lies at about 15 km depth under the continental rise, shows a variation in depth ranging from 12 to 16 km under the mid slope and reaches to a depth of about 12 km below the shelf. The velocity just below this interface (top of the crust) shows considerable variations. It is highest at 6.9 km/s under the continental rise but is generally around 6 km/s or lower under the slope and the shelf, marking a transition from the oceanic crust to the south to the continental crust to the north.

Upper mantle velocities are observed at most OBS's on Lines 5 and 3. The observed velocities are rather high at 8.4 km/s on Line 5 and 8.3 km/s on Line 3. The depth to the Moho is at about 20 km under Line 5 on the rise and at about 18 km under Line 3 in the mid slope. Although we were unable to observe mantle arrivals under other lines, the lower crustal velocities observed at significant depths indicate that the Moho to be deeper: at least 23 km below Lines 4 on the outer slope, at least 25 km below Line 2 on the upper slope and even deeper under Line 1 on the shelf. The result, therefore, shows an unusual variation in crustal thickness from the typically oceanic thickness of about 5 km under the rise to at least 7-8 km under the outer slope and down to about 5 km below the mid slope before thickening to greater than 15 km under the shelf.

The irregular variations of both the crustal velocity and thickness suggest a rather unusual transitional crust under this part of the northern Gulf. The thin crust under the mid slope may indicate this to be the site of an incipient spreading center that failed to materialize when the Gulf of Mexico opened. More studies covering adjacent areas are needed, however, to test such a hypothesis.

The shallow structural results of the present study are in fairly good agreement with those of the earlier conventional refraction surveys by *Ewing et al* [1960] and *Antoine and Ewing* [1963], which covered roughly the same area as the present experiment. Their studies, however, penetrated only down to a 7.2 km/s layer at a depth of about 15 km under the continental rise, to a 5.3 km/s layer at a depth of about 5-7 km under the mid slope and to a 5.2-5.7 km/s layer at a depth of 10-13 km under the shelf. In contrast, our data clearly depict structures significantly deeper than these, thus successfully mapping the extension of the transitional crust underlying the thick sediments.

Discussion of Some Detailed Analyses

Tau-p Inversion

The high-spatial-density data of this experiment covering a wide range of offsets can be successfully transformed from the time-distance domain of the original data into the intercept-time-ray-parameter (tau-p) domain. Assuming the structure to be one dimensional, the data then can be inverted to obtain an estimate of the velocity-depth function. We used both the extremal inversion method [*Garmany*, 1979; *Garmany et al*, 1979], wherein the range of possible depth values for given velocities is calculated, and the tau-sum method [*Diebold and Stoffa*, 1981], in which most likely velocity-depth function is estimated.

In Fig. 14, tau-p inversion results for OBS 2 of Line 5 (see Fig. 6 for the tau-p record section) are compared with a conventional layer solution based on refracted arrivals and with an interval-velocity profile obtained from the reflection moveout. The agreement among various methods is excellent for depths of less than 10 km. For depths below 10 km, the gross features are still preserved, including the velocity increases at the sediment/basement interface at about 15 km depth and the Moho at about 20 km depth. The tau-p methods are more sensitive to velocity gradients than velocity discontinuities. This contrasts with all the other 1-D methods employed in this study.

Estimation of Salt Thickness

When a mass of allochthonous salt exists at a shallow depth below an OBS, as in Line 4, the OBS record section shows the following characteristic features: a high-amplitude refracted arrival through the salt is prominently observed; the arrival time of the salt refraction is often non-linear with distance; the salt refraction stops abruptly at a certain offset distance; and after the salt arrival, there is a significant delay before arrivals from deeper layers are observed. The abrupt ending of the salt refraction and the delay of the deeper arrivals are best interpreted as resulting from the finite thickness of high-velocity salt underlain by a thick layer of low-velocity clastic sediments. These features, then, can be used to estimate the thicknesses of the salt and the layer underneath.

Two structural models shown in Fig. 15 illustrate how the thickness of the salt affects the above observed features. Each of the models consists, from the top to the bottom, of a 2 km thick water layer, low-velocity sediment down to a depth of 2.5 km, a 1- or 2-km thick salt layer with velocity varying from 4.25 km/s at the top to 4.6 km/s at the bottom, a low-velocity zone (LVZ) and a high-velocity bottom layer. Theoretical travel times of various arrivals through the models are shown in the right half of the figure. The difference between the models is clear. The salt refraction from the 1 km thick salt (upper figure) stops at about 12 km distance, while that from the 2-km thick salt (lower figure) extends to about 22 km distance. The first arrival beyond the salt refraction for either model is the reflection from the interface between the LVZ and the high-velocity bottom layer. The amount of delay after the salt refraction varies with the thickness and velocity of the LVZ. Refractions from the bottom layer are not observed till much larger offsets.

In constructing models for ray tracing, therefore, we primarily considered these features. In further refining the model, we also took into account such other factors as

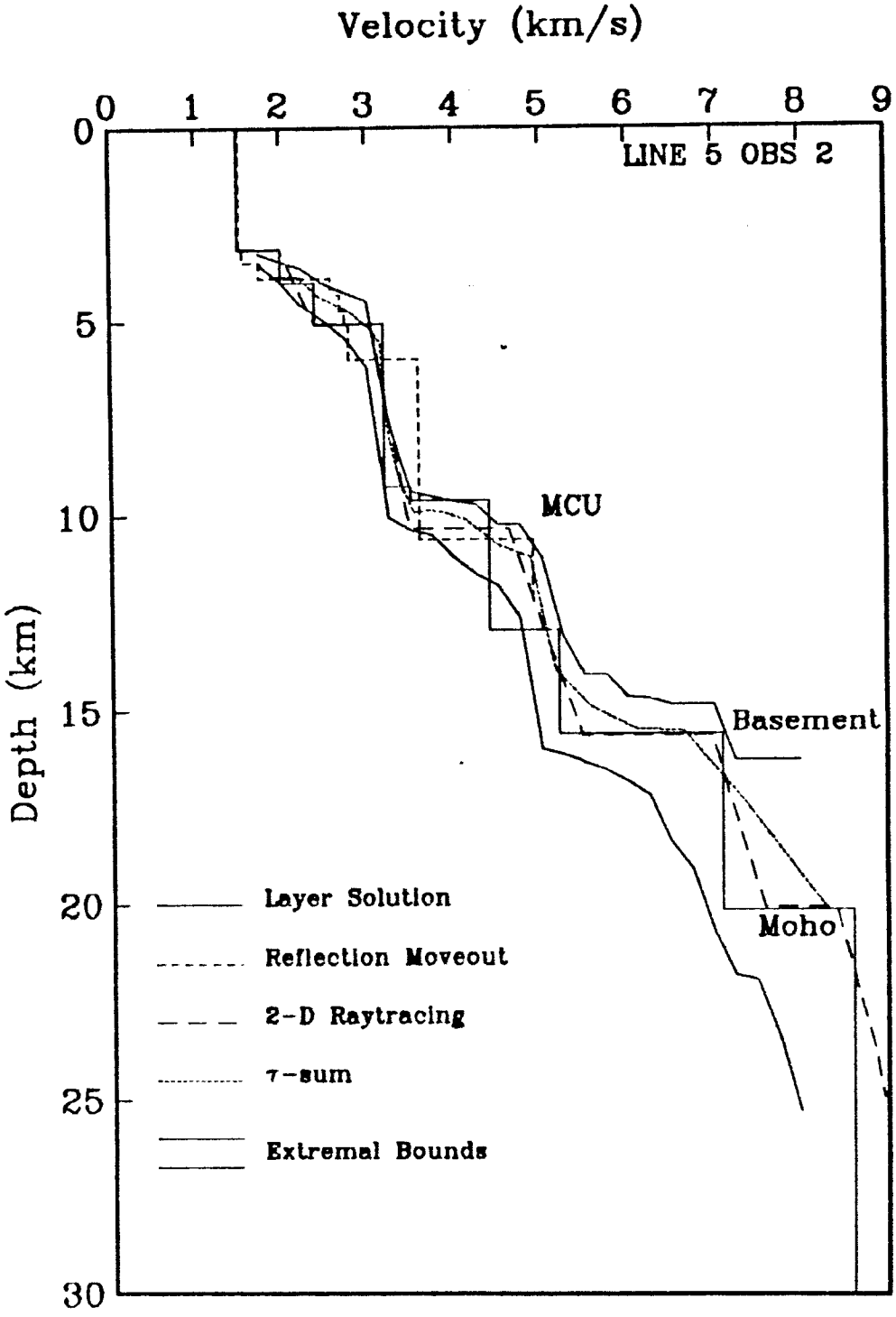

Fig. 14. Comparison of results from various 1-D velocity inversion methods

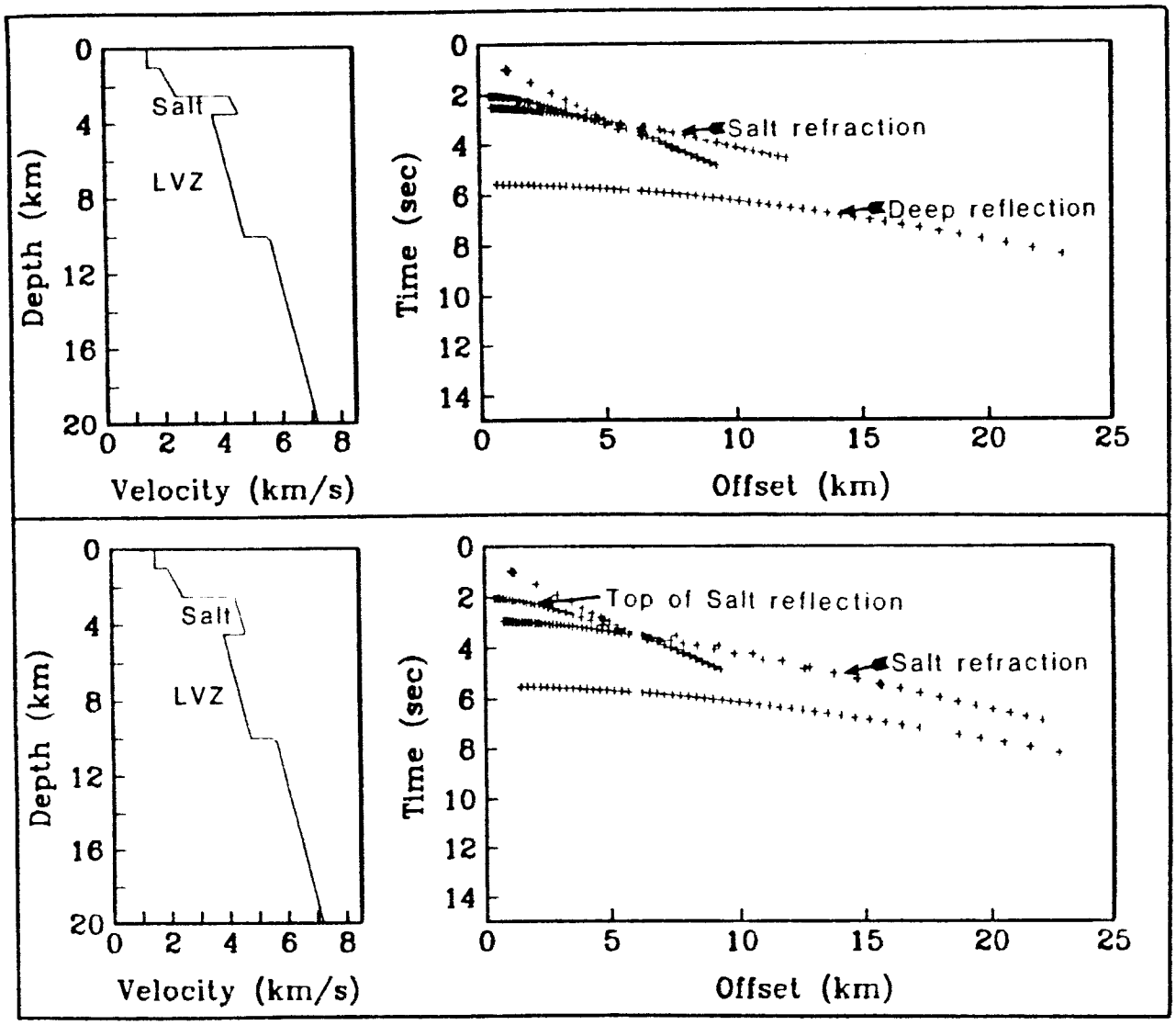

Fig. 15. Two velocity models with a shallow salt layer; one with a 1 km thick salt layer (top), and another with a 2 km thick salt layer (bottom). Note the difference in the extent of salt refractions on the travel-time-distance diagrams.

the velocity gradient in the salt and lateral variations in salt thickness, which also influenced the extent of salt refraction observation.

Generally, the interpretational problems that complex salt geometry poses are enormous. However, 2-D ray tracing based on careful consideration of various features of the record section such as discussed above provides at least a tractable method of defining both the thickness and velocity of the shallow salt. With the shallow salt structure under control, one can at last interpret with some confidence the structures further below.

Recommendations for Future Experiments

After this experiment was completed, it was clear that though the experiment was generally quite successful in revealing many structural features, there also were certain shortcomings. We list below some of these deficiencies and discuss some recommended solutions.

1. Low signal level: Using air guns for seismic signal sources has clear advantages over using explosives in terms of uniformity of source signatures, high spatial density of shot points and high accuracy of shot times. However, the signal level of individual air-gun shots is low compared with those of explosives. This is a clear limitation especially when one desires to record deep refractions through a thick, poorly consolidated sedimentary section similar to what we encountered in this study area. Besides the obvious solution of increasing the capacity of air guns, which is not always feasible technically or economically, there are many ways to improve the observed signal level from air-gun shots.

a) Finding optimum air-gun depth: -- We used 2000 cubic inch air guns towed mostly at a depth of 35 feet for this experiment. This was not only because we normally tow them at this depth for our multichannel work, but also because the bubble-pulse frequency at this depth of towing (about 6 Hz) is near the low end of the instrumental passband, which is limited by our use of 4.5 Hz geophones. Although low frequency is advantageous for long-distance transmission of seismic signals, it does not effectively utilize the surface ghost to enhance the emitted signal. Increasing the towing depth is expected to increase the bubble frequency and signal enhancement by ghost, but it also increases transmission loss. However, we have not conducted any controlled experiment to study their overall effect on signal reception at large distances. We recommend that such an experiment be done to determine the optimum depth of towing of air guns for wide-offset experiments.

b) OBS location: -- This experiment has revealed that signal strength of deep refractions is highly dependent on the bottom topography and near-surface geology. Deep refractions are generally strong when the shooting ship is over a basin or a region of well-stratified layers, but are very weak over complex salt structures. The cause of this difference may be attributable either to focusing and defocusing of seismic rays by structures or to the difference in absorption and scattering of seismic energy through different geologic structures. Whatever the reason for this difference, we will be better off locating OBS's in basins or over well-stratified structures rather than over complex salt structures whenever possible.

c) Repeated shots: -- Detection of weak seismic signals at far distances is often accomplished by correlation of arrivals across several neighboring traces. Theoretically the higher the spatial density of the sources, the better the chance of

detecting weak signals because of the increased effective signal-to-noise ratio. For the present experiment, we shot a part of each line at 50% higher spatial density than the rest. The result, however, is inconclusive. We may need a larger difference in spatial density to see the effect clearly. An extreme case will be to keep the shooting ship stationary while shooting a large number of shots at a given distance. However, we are not ready to recommend such a procedure except for experimental purposes because the additional ship time required to achieve appreciable improvement in the signal-to-noise ratio is quite significant and may even be uneconomical.

d) Multiple OBS's at one location: -- The other way to increase the data density for a better signal-to-noise ratio is to deploy more than one OBS at a given location. Assuming that they are separated by a distance sufficient to have independent background noise but close enough to detect essentially the same distant arrivals, we should be able to achieve significant improvement in signal-to-noise ratio.

e) Geophone selection: -- We have not yet conducted any controlled experiment to determine the relative contributions of various possible sources of noise to the overall background noise. If the noise generated at the geophone is significant, and we have a reason to believe it may be, selection of geophones with higher output and larger suspended mass may improve the overall signal-to-noise ratio. We recommend that we examine various possible sources of noise to see if some of them may be controllable.

2. Line geometry: Unless the structure is nearly flat in all directions, the orientation of the shooting line and OBS locations are very important in acquiring readily interpretable data. In areas of large lateral heterogeneities, reflections and refractions from features off the shooting line may significantly influence the observation. Fortunately, since each OBS is completely detached from the shooting ship, there is no problem in deploying some OBS's off the shooting line. Off-line OBS's will help remove ambiguities of interpretation due to structural variations perpendicular to the shooting line. If appropriate, non-linear shooting geometry may also be adopted to further enhance the lateral control. For future experiments, it is recommended that due consideration be given to the most appropriate geometry for shooting lines and OBS locations.

3. Data analysis techniques: Though we have found it most successful to use 2-D ray tracing in dealing with complex structures like those found in this study area, the technique is non-unique, and the resulting structure may not be a correct one. One way to test the validity of the derived structure is to compare synthetic seismograms based on the derived model to the observations. Therefore, we recommend that such an approach be developed for use in future studies.

Conclusions

The present experiment using OBS's, air guns and modern data analysis techniques to study the deep crustal structure of the northern Gulf of Mexico has revealed, for the first time, the basement and lower crustal structure across this continental margin. The new findings are :

1. The entire study area from the shelf to the continental rise is covered with a thick (13-15 km) sedimentary sequence.

2. The salt features found under the slope range from mostly deep-seated salt with diapirs under the inner slope to shallow but relatively thin allochthonous salt bodies under the outer slope.

3. The middle Cretaceous unconformity, at about 11 km depth under the continental rise, shows a gentle rise in section through the slope to about 9 km depth under the shelf.

4. The depth to the crystalline basement, about 15 km under the continental rise, shows an oscillatory variation under the slope and reaches about 12 km under the shelf.

5. The Moho is found at a depth of about 20 km under the continental rise and deepens under the outer slope. However it becomes quite shallow at about 18 km depth below the mid slope before it deepens again below the shelf.

6. Consequently, the crustal thickness shows an unusual variation: from the typical oceanic thickness of about 5 km under the rise to at least 7-8 km under the outer slope and down to about 5 km again under the mid slope before thickening to greater than 15 km under the shelf.

7. The crustal velocity also shows considerable lateral variation: just below the sediments, it varies from 6.9 km/s under the continental rise to around 6 km/s or lower under the slope and the shelf.

8. The irregular variations of both the crustal velocity and thickness suggest a non-uniform extension of this continental margin at the time of the formation of the Gulf of Mexico basin.

Acknowledgements . This project was conceived by a group of scientists at the Institute for Geophysics lead by Arthur E. Maxwell and at the U. G. Geological Survey, Woods Hole. We appreciate Dr. Maxwell's interest and encouragement throughout this study. The ocean-bottom seismographs used for the experiment were designed principally by Paul L. Donoho, now with Chevron Oilfield Research Co., working under the direction of Gary V. Latham, now with Cities Service. Phillip H. Roper, Paul M. McPherson and Michael Butterfield were responsible for building, maintaining and operating the instruments as well as many other related mechanical, electronic and programming tasks. Captain Bruce H. Collins of R/V *Fred H. Moore* and his crew were extremely helpful in making this experiment successful. Kenneth H. Griffiths, Patricia E. Ganey, Julie McEuen, Subir Chatterjee, George W. Pearcy, Stirling Gilfillan, Oscar Febres-Cordero, Christopher Bennett and Thomas Davies were responsible for many ship-related operations including electronics, mechanical work, navigation, data acquisition and communication. The 2-D ray tracing program used in this study was developed by Kevin MacKenzie based on the original program of V. Cerveny.

REFERENCES

Antoine, J. and J. Ewing, Seismic refraction measurements on the margins of the Gulf of Mexico, *J. Geophys. Res., 68*, 1975-1996, 1963.

Buffler, R. T., *Seismic Stratigrtaphy and Geologic History of the Deep Gulf of Mexico Basin and Adjacent Margins* 306 pp., Professional Seminar Group, Houston, 1984.

Buffler, R. T., J. L. Worzel and J. S. Watkins, Deformation and origin of the Sigsbee scarp - lower continental slope, northern Gulf of Mexico, *Offshore Tech. Conf. 3*, OTC 3217, 1425-1433, 1978.

Diebold, J. B. and P. L. Stoffa, The travel time equation, tau-p mapping and inversion of common midpoint data, *Geophysics, 46*, 238-354, 1981.

Ewing, J., J. Antoine and M. Ewing, Geophysical measurements in the western Caribbean Sea and in the Gulf of Mexico, *J. Geophys. Res., 65*, 4087-4126, 1960.

Garmany, J. D., On the inversion of travel times, *Geophys. Res. Lett., 6*, 277-280, 1979.

Garmany, J., J. A. Orcutt, and R. L. Parker, Travel time inversion: A geometrical approach, *J. Geophys. Res., 84*, 3615-3622, 1979.

Papadakes, E. S., Attenuation of pure elastic modes in NaCl single crystals, *Appl. Phys., 34*, 1872, 1963.

Pilger, R. H., Jr. and M. T. Angelich, Gravity Anomalies, in *Ocean Margin Drilling Program Regional Atlas Series, Atlas 6, Gulf of Mexico*, edited by R. T. Buffler, S. D. Locker, W. R. Bryant, S. A. Hall and R. H. Pilger, Jr., Sheet 2, Marine Science International, Woods Hole, 1984.

Stoffa, P. L., P. Buhl, J. B. Diebold, and F. Wenzel, Direct mapping of seismic data to the domain of intercept time and ray parameter – A plane wave decomposition, *Geophysics, 46*, 255-267, 1981.

Worzel, J. L. and W. R. Bryant, Regional aspect of deep sea drilling of the Gulf of Mexico, Leg 10, in *Initial Reports of the Deep Sea Drilling Projects, 10*, pp. 737-748, U. S. Government Printing Office, Washington, 1973.